HHS Public Access

Author manuscript

Ultrasound Med Biol. Author manuscript; available in PMC 2020 July 01.

Published in final edited form as:

Ultrasound Med Biol. 2019 July ; 45(7): 1850–1856. doi:10.1016/j.ultrasmedbio.2019.03.009.

Virtual Brain Projection for Evaluating Trans-Skull Beam Behavior of Transcranial Ultrasound Devices

Spencer T. Brinker[1], **Frank Preiswerk**[1], **Nathan J. McDannold**[1], **Krystal L. Parker**[2], **Timothy Y. Mariano**[3,4]

[1]Department of Radiology, Brigham & Women's Hospital, Harvard Medical School, Boston, U.S.A.

[2]Carver College of Medicine, The University of Iowa, Iowa City, IA, USA

[3]Department of Psychiatry, Brigham & Women's Hospital, Harvard Medical School, Boston, U.S.A

[4]Butler Hospital, Providence, RI, USA

Abstract

Focused ultrasound (FUS) single-element piezoelectric transducers (SEPTs) are a promising method to deliver ultrasound to the brain in low-intensity applications, but experiences defocusing and high-attenuation due to transmission through the skull. Here, a novel virtual brain projection method is used to superimpose a magnetic resonance imaging (MRI) brain within ex-vivo human skulls to provide targets during trans-skull FUS SEPT pressure field mapping. Positions of the transducer, skull, and hydrophone are tracked in real-time using a stereoscopic navigation camera and 3D-Slicer software. Virtual targets of left dorsolateral prefrontal cortex (DLPFC), left hippocampus (HPC), and cerebellar vermis (CBM-VER) were chosen for demonstrating the method's flexibility to evaluate focal-zone beam distortion and attenuation. The regions are of interest as non-invasive brain stimulation (NIBS) targets to treat neuropsychiatric disorders via repeated ultrasound exposure. The technical approach can facilitate the assessment of transcranial ultrasound device operator positioning reliability, intracranial beam behavior, and computational model validation.

Keywords

Virtual brain projection; Transcranial ultrasound; Dorsolateral prefrontal cortex; Hippocampus; Cerebellar vermis

Introduction

Single-element piezoelectric transducers (SEPTs) in combination with neuronavigation systems have recently been used in several human investigations to transmit Pulsed low-

Corresponding Author: Spencer T. Brinker, Postal Address: 221 Longwood Avenue, EBRC 521 Boston, MA 02115, Phone number: 309-303-8459, spencer.t.brinker@gmail.com.

intensity focused ultrasound (PLIFU) through the skull. Cortical and subcortical regions including the occipital lobe, frontal lobe, and thalamus have been targeted to suppress evoked potentials in healthy human volunteers with no adverse effects reported (Lee et al. 2016b; Lee et al. 2016a; Legon et al. 2018). FUS parameters used in these studies were in some cases above FDA limits for diagnostic ultrasound (Duck 2007) (Spatial Peak Temporal Average Intensity (I_{sppa}) = 190 W/cm^2 and Spatial Peak Temporal Average Intensity (I_{spta}) = 0.75 W/cm^2) but were still within range of the Electrotechnical Commission limit for therapeutic ultrasound (I_{spta} = 3 W/cm^2) (Duck 2007). In addition to these regulatory limits, clinical data has recently become available to better understand thermal and cavitation effects of FUS on brain tissue in the high-intensity regime (McDannold et al., 2010), which in turn has aided investigators conducting low-intensity studies to design FUS parameters that minimize tissue heating and cavitation for avoiding tissue damage. FUS has recently been shown to safely open the Blood Brain Barrier (BBB) in humans using a hemispherical phased-array transducer (Lipsman et al. 2018). Preclinical studies have also shown success in using neuronavigation-guided SEPT's to open the BBB (Wei et al. 2013; Wu et al. 2018).

However, the FUS beam behavior of SEPTs drastically changes depending on the FUS target location and skull entrance position as is demonstrated in the preliminary experimental results of this investigation. The need to conduct safety pretests is apparent when assessing the results of a prior human study using an unfocused ultrasound emitter, which caused subcarotid space hemorrhage in two patients (Tsivgoulis and Alexandrov 2007). It was later estimated using computational modeling that unforeseen side lobes of high intensities accumulated at the skull interface within the near-field of the FUS beam, causing the adverse events. Computer modeling is valuable when using subject-specific images in semi-real-time analysis for steering FUS beams to new locations for attenuation estimation, defocusing correction, and possible warnings of undesired standing wave formations (Yoon et al. 2018). The porous microstructure and curvature of skull tissue has a major impact on the amount of attenuation a FUS beam experiences while being transmitted through the skull, which computational modeling cannot totally account for given the limited spatial resolution of X-ray computed tomography used in the modeling.

Direct physical measurements with hydrophone scanning have been used to evaluate the FUS beam as it travels through human skull specimens (Ammi et al. 2016; Korb et al. 2014; Lee et al. 2015; Legon et al. 2014; Marsac et al. 2017; White et al. 2006) and in some cases these were complimented by computational modeling. The measurements yielded estimates of FUS power loss in correlation with skull bone thickness (SBT) within the beam path but the investigation did not include pointing the FUS device beam towards specific brain targets. The intent of our virtual brain projection method is thus to collect actual beam attenuation and defocusing data when SEPTs or other FUS devices are aimed towards specific human brain regions that may be putative targets for NIBS treatment of major depression, epilepsy, and other neuropsychiatric disorders. Our method is of relevance for evaluating transcranial FUS devices for these potential FUS treatments since it can assess, with empirical data, how well an operator can put a transcranial FUS beam on a target using neuronavigation guidance. The gold standard for using FUS SEPTs in target-specific transcranial applications is neuronavigation via optical tracking. A device operator solely relies on where the crosshairs of the beam's focal area are overlaid onto a subject's pre-

procedure MRI as displayed on a computer screen during FUS sonication. The method adds the factor of device operator positioning error into the treatment evaluation, which a computational model cannot achieve alone.

Material and Methods

The hardware for conducting the virtual brain projection employed an automated 3D positioning system (MB603601J-S6, Velmex Inc., Bloomfield, NY), hydrophone (HNC-0400, Onda CorpHNC-0400, Sunnyvale, CA), oscilloscope (DPO 3034, Tektronix, Beaverton, OR), function generator (33220A, Agilent Technologies, Santa Clara, CA), RF amplifier (240L; Electronics & Innovation, Ltd., Rochester, NY), two custom air-backed SEPTs (272 kHz, both 5 cm dimeter, with 3.25 and 7.5 cm focal lengths), stereoscopic neuronavigation camera (Polaris Vicra, Northern Digital Inc., Ontario, Canada), and custom optical trackers. A Windows personal computer running 3D Slicer (version 4.8.1) (Fedorov et al. 2012), Plus Toolkit (version 2.6.0.20180310) (Lasso et al. 2014), and (The MathWorks Inc., Natick, MA, USA) was used to control the experimental platform (Fig. 1). Before pressure field scans were acquired, two adult human skull specimens (preserved in formalin (calvaria and the left portion of a parasagittally sectioned skull, skull gender and age at death unknown) previously stored in formalin were each fitted with five donut-shaped fiducial markers (PinPoint#128, Beekley Medical, Bristol, CT) at arbitrary positions. The specimens were scanned with pointwise encoding time reduction pulse sequence with radial acquisition in a 3T MRI scanner (Magnetrom Skyra, Siemens Corp, Munich, Germany), which is sensitive to bone contrast. MRI parameters for each skull were echo time = 0.07 s, repetition time = 3.61 s, coronal slices, 1 mm isotropic resolution, 1 average; scan time was approximately 15 minutes. Skulls were removed from formalin and rinsed with water and dried with paper towels; then fiducials were placed on skulls and the unsubmerged skulls were held in place within a head RF coil for scanning. A permanent marker was used to indicate the center locations of the fiducial on the specimens before the fiducials were removed.

Each skull specimen’s image volume was separately processed using 3D Slicer’s Landmark Registration module to merge a healthy standard brain MRI imaging volume into the specimen volumes. The specimen and brain MRI were set to fixed volume and moving volume, respectively, for the registration process. The transformed MR image and the specimen image volumes were added into one image volume. Affine registration and manually placed landmarks were used to merge the brain with the calvaria whereas automatic thin plate spline registration was used for merging the parasagittally sectioned specimen. Both specimens filled with the virtual brain were saved as separate 3D Slicer scenes. The scenes contain a hierarchy of reference frames representing the spatial locations of each tracked item in the camera’s optical field of view. The Plus Toolkit was used to interface with the optical tracking camera. All transforms were sent to 3D Slicer in real-time using the OpenIGTLink network protocol (Tokuda et al. 2010).

FUS pressure field mapping was conducted in a tank filled with degassed and deionized water. Optical Trackers (OT) were rigidly fixed to transducer, specimen, and the positioning system rod attached to the hydrophone. A custom Optical Tracking Pointer (OTP) was used

to register each OT to the spatial locations of the transducer, FUS focus, hydrophone tip, and skull in the optical tracking camera's coordinate system. The spatial location of each item could then be tracked in real-time within the 3D Slicer user interface window. Coronal, sagittal, axial, and isometric views of the virtual brain/skull are set as a static reference frame in the window, therefore allowing transducer and hydrophone movements to be observed as the skull remains stationary in the window.

The hydrophone was positioned perpendicular to the transducer's emitting surface while keeping both orthogonal to the automated 3D positioning system. The skull specimen was then positioned so the FUS focus was aligned with the virtual brain target while the transducer was oriented perpendicular to the skull surface. The transducer and skull specimens were held by ring stands. All alignment procedures in this proof-of-concept study were approximated by visual line of sight. FUS parameters used during pressure mapping were 272 kHz sine wave in burst mode, 10 cycles, 20 ms burst period, and approximately 100 mW acoustic power. Axial and longitudinal pressure mapping with 1 × 1 mm pixel resolution was performed in the FUS focus region both with and without the skull. The calvaria specimen was used to target the virtual left DLPFC with multiple mapping planes along the FUS focus to demonstrate the virtual brain projection method using the 3.25 cm focal length transducer. parasagittally sectioned skull specimen was used for virtual left HPC and left portion of the CBM-VER using the 7.25 cm focal length transducer. These virtual targets were selected as a preliminary investigation of FUS propagation in brain regions of interest to NIBS investigations to treat neuropsychiatric disorders. SBT in the FUS path was approximated by taking measurements from the skull specimens using large curved outside caliper (Lufkin, Sparks, MD, USA) and a digital linear caliper (CD-6" CS, Mitutoyo Corp., Kawasaki, Japan) (White et al. 2006), with an accuracy of approximately ± 0.5 mm. A spatial peak pressure reduction (SPPR) (1) was calculated for estimating the acoustic pressure loss while transmitting ultrasound through the skull. Normalized spatial peak pressure (SPP) is acquired from the axial pressure images without skull obstruction in the FUS beam and with skull obstruction and represented as SPP_{ns} and SPP_s, respectively.

$$SPPR = \left(1 - \frac{SPP_s}{SPP_{ns}}\right) x\, 100 \quad (1)$$

Results

The FUS pressure field maps acquired while targeting the virtual left DLPFC are shown in Fig. 2. Axial and longitudinal scans are shown at various locations in the FUS focal region. Attenuation depends on the subject-specific SBT, which changed with each brain target. The left DLPFC SBT ≈ 9 mm (frontal bone) correlated with an SPPR = 18.2 % as the FUS was transmitted through the calvaria specimen. Fig. 3 and Fig. 4 show preliminary scans to investigate how the FUS beam behaves as it travels through the bone to virtual targets HPC (SPPR = 56.9 %, SBT ≈ 4 mm temporal bone, ≈ 7.5 mm anterior parietal bone, ≈ 5.5 mm posterior parietal bone) and CBM-VER (SPPR = 69.6 %, SBT ≈ 8 mm occipital bone), respectively.

Discussion and Summary

Our proof-of-concept study demonstrates how this novel virtual brain projection method is a practical approach for investigating FUS trans-skull beam behavior of transcranial ultrasound devices before conducting in-vivo preclinical and clinical investigations. Human brain targets can be chosen to optimize FUS device beam parameters and verify the efficacy of the ultrasound propagation mechanics relative to the brain region of interest. Several such regions of value to NIBS researchers were selected. The transducers were chosen specially so their focal zone could reach the depth of the targets. Our method allowed us to visualize if the distorted focal-zone of the longitudinal pressure map reaches the inner layer of the skull. This is important to achieve since the FUS energy should be directed away from the skull to minimize skull heating. We could also visualize how the distorted focal-zone in both pressure fields maps reaches beyond the neuronavigation crosshairs.

The experimental workflow presented was conceived during the development of a custom human nueronavigation-guided FUS SEPT system to transmit ultrasound energy incrementally to a participant's entire hippocampus during a multi-session course of treatment. It was decided to evaluate the focal-zone distortion and attenuation using the method described here--instead of via computational modeling--since our method obtains empirical data in a scenario similar to real-world experimental/clinical conditions. By using PLIFU stimulations at low duty cycles along with interstimulus intervals and acoustic intensities known to be safe in prior human studies, we assumed near-field beam standing waves and skull heating can be avoided, respectively without a comprehensive computational modeling.

Dorsolateral Prefrontal Cortex

The left DLPFC has traditionally been the cortical target for the FDA-approved use of repetitive transcranial magnetic stimulation (rTMS) for successful treatment of major depressive disorder symptoms (Carpenter et al. 2012; Rosa and Lisanby 2012). In current clinical practice, placement of the coil utilizes a rule-of-thumb (Carpenter et al. 2012) that can be imprecise. Commercial neuronavigation systems have gained some popularity for increased precision in rTMS treatment, but such systems remain costly. Low-intensity transcranial ultrasound may offer an attractive alternative to rTMS as an NIBS strategy to treat depression (Bowary and Greenberg 2018; Tsai 2015) and has been used to modulate right inferior frontal gyrus, showing improvements in mood and alterations of functional connectivity (Sanguinetti et al. 2017). SEPT FUS may have a higher spatial targeting capability compared to TMS. The results in Fig. 2 show that delivering FUS through the calvaria produces only moderate defocusing when targeting the left DLPFC.

Hippocampus

Since rTMS is generally only used to target superficial cortical structures, it is difficult to target HPC for NIBS. Attempts have been made with figure eight and other TMS coil configurations to stimulate deep temporal lobe regions in humans and were able to reach depths within 6 cm of the skull but still lacked focality (Gersner et al. 2016; Sun et al. 2012) to target the HPC selectively. PLIFU NIBS via SEPTs to target the HPC has been shown to

potentially cause neuromodulation effects. A previous study shows PLIFU stimulation can alter electrically evoked responses in rat hippocampal slices using a SEPT (Rinaldi et al. 1991). PLIFU stimulation has also shown some indication of suppressing seizure activity in animal models (Min et al. 2011). However, the benchtop testing did not investigate the technical feasibility of transmitting ultrasound through the skull in a human application.

The pressure field maps in Fig. 3 are intended to demonstrate the virtual brain projection technique's ability to mimic a HPC target in a parasagittally sectioned skull specimen. It appears the FUS focus is tightened longitudinally and the FUS focal center is redirected off center in the axial direction. To draw important conclusions about HPC targeting, one would have to conduct a more thorough investigation using this platform and computational modeling. Targeting multiple portions of the HPC with a SEPT would require beam entry through the parietal and squamous structure of the temporal bone. Determining the average SBT a FUS is transmitted through the squamous structure line is complicated since the area has variable bone thickness. A simplified method for determining the FUS intensity needed to transmit ultrasound through the skull based on SBT alone is not yet a standard in the FUS research community but needs to be addressed as SEPT may need to meet future regulatory intensity limits for therapeutic ultrasound in the brain. The results from our demonstration experiments indicate there is not a general linear correlation between SBT and SPPR throughout the brain targets. This is likely caused by differences in skull curvature and bone porosity attenuation affects. SPPR can be affected by the incidence angle of ultrasound propagation through the skull (White et al. 2006). Here, all experiments used a best line-of-sight while aligning the traducer normal to the skull to minimize this affect.

Cerebellum

A growing area of NIBS research involves extra-cortical targets such as the cerebellum, a structure traditionally exclusively associated with motor control; however, recent work has demonstrated the cerebellum's role in cognitive and affective processes (Walsh and Parker 2018). Thus, it may be a novel therapeutic target for neuropsychiatric disease due to its ability to modulate frontal and prefrontal cortical function. Experimental work in human participants has shown that stimulation of the cerebellum including via rTMS and theta-burst TMS can reduce seizure frequency in epileptic patients, relieve cognitive symptoms of schizophrenia, and improve mood in treatment resistant depression (Walsh and Parker 2018). However, a major drawback of rTMS is its relative inability to stimulate brain structures not near the cortical surface; for example, when considering deep brain targets of relevance to chronic pain and other neuropsychiatric disorders, current neuromodulation methods providing both depth and focality are invasive, such as deep brain stimulation (Boccard et al. 2014; Boccard et al. 2017). Similarly, the small size of sub-cerebellar targets, access difficulty to these areas with modalities like TMS, and other anatomical considerations present challenges for the promising research area of cerebellar NIBS. PLIFU may ultimately be able to address these problems (Fig 4), although the defocusing and attenuation noted in the FUS pressure field maps so indicate that additional study is needed. More experiments for obtaining pressure measurements through a larger number of skulls must be performed in order to determine inter-patient attenuation and aberrations variation.

Limitations and Future Directions

This technique is a helpful tool for preliminary evaluation of SEPT devices for use in transcranial FUS applications, but there are some technical limitations using this technique. Alone, our method does not provide full device safety or efficacy evaluation, such as skull heating, near-field standing waves, full beam distortion quantification analysis, and neurophysiological effects of the modality; these would require additional experimental and computational methods. A beneficial attribute of the system is its capability to replicate the position of the transducer and ex-vivo skull specimen used in a computational model. This could facilitate the empirical validation of the computer-generated FUS beam focal-zone distortion and attenuation.

Also, hydrophone mapping is limited to measurement no nearer than a few millimeters from the skull surface, as otherwise damage may occur to the hydrophone tip from collision with the inner skull surface, particularly when visual line of sight is limited. The OPT was used to mark the location of the hydrophone tip to define reference points in virtual target regions of interest. Tracking the tip positions in the navigation software window was helpful when setting the boundary limits of the automated 3D positioning system. It may be beneficial to mark reference locations of the FUS beam pressure maps, transducer, and skull so their experimental positions could be fitted into a computational geometry for further investigation of the FUS beam propagation using computational modeling.

In addition, the method could be used to empirically optimize and evaluate prospective non-neuronavigation-guided transcranial ultrasound devices indented to target a specific area of the brain during the device development stages. Some device examples being transcranial Doppler imaging probes (Sanguinetti et al. 2017), spherical phased arrays (Leinenga et al. 2016), or flat face SEPTs (Barlinn et al. 2013), which have been proposed or used in past human NIBS investigations. The virtual brain projection platform could be used to empirically validate device design parameters such as SEPT lens geometries, phased array aberration correction parameters, or electronic beam steering strategies. Human MRI brain volumes of tumors or other disease related structures could be used in place of the healthy virtual brain to investigate FUS beam propagations to other application of interest. Our proof-of-concept study provides new insight for the potential use of neuronavigation-guided SEPT PLIFU stimulation for NIBS of cortical targets relevant to multiple human neuropsychiatric disorders.

Acknowledgments

This work was supported by the National Institutes of Health under grant P01CA174645 and R25CA089017.

References

Ammi AY, Mast TD, Huang I, Abruzzo TA. Characterization of Ultrasound Propagation Through Ex-vivo Human Temporal Bone. Ultrasound Med Bio 2016;34:1578–1589.

Barlinn K, Barreto AD, Sisson A, Liebeskind DS, Schafer ME, Alleman J, Zhao L, Shen L, Cava LF, Rahbar MH, Grotta JC, Alexandrov AV. CLOTBUST-Hands Free Initial Safety Testing of a Novel Operator-Independent Ultrasound Device Device in Stroke-Free Volunteers. Stroke 2013;1641–1647. [PubMed: 23598523]

Boccard SGJ, Fitzgerald JJ, Pereira EAC, Moir L, Van Hartevelt TJ, Kringelbach ML, Green AL, Aziz TZ. Targeting the affective component of chronic pain: A case series of deep brain stimulation of the anterior cingulate cortex. Neurosurgery 2014;74:628–635. [PubMed: 24739362]

Boccard SGJ, Prangnell SJ, Pycroft L, Cheeran B, Moir L, Pereira EAC, Fitzgerald JJ, Green AL, Aziz TZ. Long-Term Results of Deep Brain Stimulation of the Anterior Cingulate Cortex for Neuropathic Pain World Neurosurg Elsevier Inc, 2017;106:625–637. [PubMed: 28710048]

Bowary P, Greenberg B. Noninvasive Focused Ultrasound for Neuromodulation: A Review. Psychiatr Clin 2018;41:505–514.

Carpenter LL, Janicak PG, Aaronson ST, Boyadjis T, Brock DG, Cook IA, Dunner DL, Lanocha K, Solvason HB, Demitrack MA. Transcranial magnetic stimulation (TMS) for major depression: A multisite, naturalistic, observational study of acute treatment outcomes in clinical practice. Depress Anxiety 2012;29:587–596. [PubMed: 22689344]

Duck FA. Medical and non-medical protection standards for ultrasound and infrasound. Pog Biophys Mol Biol 2007;93:176–191.

Fedorov A, Beichel R, Kalphaty-Cramer J, Finet J, Fillion-Robbin J-C, Pujol S, Bauer C, Jennings D, Fennessy F, Sonka M, Buatti J, Aylward S, Miller JV, Pieper S, Kikinis R. 3D slicers as an image computing platform for thw quantitative imaging network. Magn Reson Imaging 2012;30:1323–1341. [PubMed: 22770690]

Gersner R, Oberman L, Sanchez MJ, Chiriboga N, Kaye HL, Pascual-Leone A, Libenson M, Roth Y, Zangen A, Rotenberg A. H-coil repetitive transcranial magnetic stimulation for treatment of temporal lobe epilepsy: A case report Epilepsy Behav Case Reports Elsevier B.V., 2016;5:52–56.

Korb AS, Shellock FG, Cohen MS, Bystritsky A. Low-Intensity Focused Ultrasound Pulsation Device Used During Magnetic Resonance Imaging : Evaluation of Magnetic Resonance Imaging-Related Heating at 3 Tesla / 128 MHz. 2014;2013:236–241.

Lasso A, Heffter T, Rankin A, Pinter C, Ungi T, Fichtinger G. PLUS: open-source toolkit for ultrasound-guided intervention systems. 2014;61:2527–2537.

Lee W, Chung YA, Jung Y, Song IU, Yoo SS. Simultaneous acoustic stimulation of human primary and secondary somatosensory cortices using transcranial focused ultrasound. BMC Neurosci BioMed Central, 2016a;17:1–11.

Lee W, Kim H, Jung Y, Chung YA, Song I, Lee J. Transcranial focused ultrasound stimulation of human primary visual cortex. Nat Publ Gr Nature Publishing Group, 2016b;:1–12.

Lee W, Kim H, Jung Y, Song I, Chung YA, Yoo S. Image-Guided Transcranial Focused Ultrasound Stimulates Human Primary Somatosensory Cortex. Sci Rep 2015;5:1–10.

Legon W, Ai L, Bansal P, Mueller JK. Neuromodulation with single-element transcranial focused ultrasound in human thalamus. Hum Brain Mapp 2018;39:1995–2006. [PubMed: 29380485]

Legon W, Sato TF, Opitz A, Mueller J, Barbour A, Williams A, Tyler WJ. Transcranial focused ultrasound modulates the activity of primary somatosensory cortex in humans. Nat Publ Gr Nature Publishing Group, 2014;17:322–329.

Leinenga G, Langton C, Nisbet R, Götz J. Ultrasound treatment of neurological diseases — current and emerging applications. Nat Rev Neurol 2016;12:161–174. [PubMed: 26891768]

Lipsman N, Meng Y, Bethune AJ, Huang Y, Lam B, Masellis M, Herrmann N, Heyn C, Aubert I, Boutet A,Smith GS, Hynynen K, Black SE. Blood–brain barrier opening in Alzheimer's disease using MR-guided focused ultrasound. Nat Commun 2018;9:2336. [PubMed: 30046032]

Marsac L, Chauvet D, La Greca R, Boch A, Chaumoitre K, Tanter M, Aubry J. Ex vivo optimisation of a heterogeneous speed of sound model of the human skull for non-invasive transcranial focused ultrasound at 1 MHz. Int J Hyperth 2017;33:635–645.

McDannold N, Clement G, Hynynen K, Black P, Jolesz F. Transcranial MRI-guided focused ultrasound surgery of brain tumors: Initial findings in three patients. Neurosurgery 2010;66:323–332. [PubMed: 20087132]

Min B, Bystritsky A, Jung K, Fischer K, Zhang Y, Maeng L, Park SI, Chung Y, Jolesz FA, Yoo S. Focused ultrasound-mediated suppression of chemically-induced acute epileptic EEG activity BMC Neurosci BioMed Central Ltd, 2011;12:23. [PubMed: 21375781]

Rinaldi PC, Jones JP, Reines F, Price LRR. Modification by focused ultrasound pulses of electrically evoked responses from an in vitro hippocampal preparation. Brain Res 1991;558:36–42. [PubMed: 1933382]

Rosa MA, Lisanby SH. Somatic treatments for mood disorders Neuropsychopharmacology Nature Publishing Group, 2012;37:102–116. [PubMed: 21976043]

Sanguinetti JL, Hameroff S, Allen JJB. Transcranial ultrasound improves mood and affects resting state functional connectivity in healthy volunteers. Brain Stimul Basic, Transl Clin Res Neuromodulation 2017;10:426.

Sun W, Mao W, Meng X, Wang D, Qiao L, Tao W, Li L, Jia X, Han C, Fu M, Tong X, Wu X, Wang Y. Low-frequency repetitive transcranial magnetic stimulation for the treatment of refractory partial epilepsy: A controlled clinical study. Epilepsia 2012;53:1782–1789. [PubMed: 22950513]

Tokuda J, Fischer GS, Papademetris X, Yaniv Z, Cheng P, Liu H, Blevins J, Arata J, Alexandra J, Kapur T,Pieper S, Burdette EC, Fichtinger G, Clare M, Hata N. OpenIGTLink: an open network protocol for image-guided therapy environment. 2010;5:423–434.

Tsai SJ. Transcranial focused ultrasound as a possible treatment for major depression Med Hypotheses Elsevier Ltd, 2015;84:381–383. [PubMed: 25665863]

Tsivgoulis G, Alexandrov AV. Ultrasound-Enhanced Thrombolysis in Acute Ischemic Stroke: Potential, Failures, and Safety. 2007;4:420–427.

Walsh K, Parker KL. The Role of the Cerebellum in Cognitive and Affective Processes. Ref Modul Biomed Sci 2018.

Wei K, Tsai H, Lu Y, Yang H, Hua M, Wu M, Chen P, Huang C, Yen T, Liu H. Neuronavigation-Guided Focused Ultrasound-Induced Blood- Brain Barrier Opening: A Preliminary Study in Swine. AJNR Am J Neuroradiol 2013;34:115–20. [PubMed: 22723060]

White PJ, Hynynen K, Clement GT. Longitudinal and shear mode ultrasound propagation in human skull bone. Ultrasound Med Bio 2006;829:251–255.

Wu SY, Aurup C, Sanchez CS, Grondin J, Zheng W, Kamimura H, Ferrera VP, Konofagou EE. Efficient blood-brain barrier opening in primates with neuronavigation-guided ultrasound and real-time acoustic mapping. Sci Rep 2018;8:1–11. [PubMed: 29311619]

Yoon K, Lee W, Croce P, Cammalleri A, Yoo SS. Multi-resolution simulation of focused ultrasound propagation through ovine skull from a single-element transducer Phys Med Biol IOP Publishing, 2018;63.

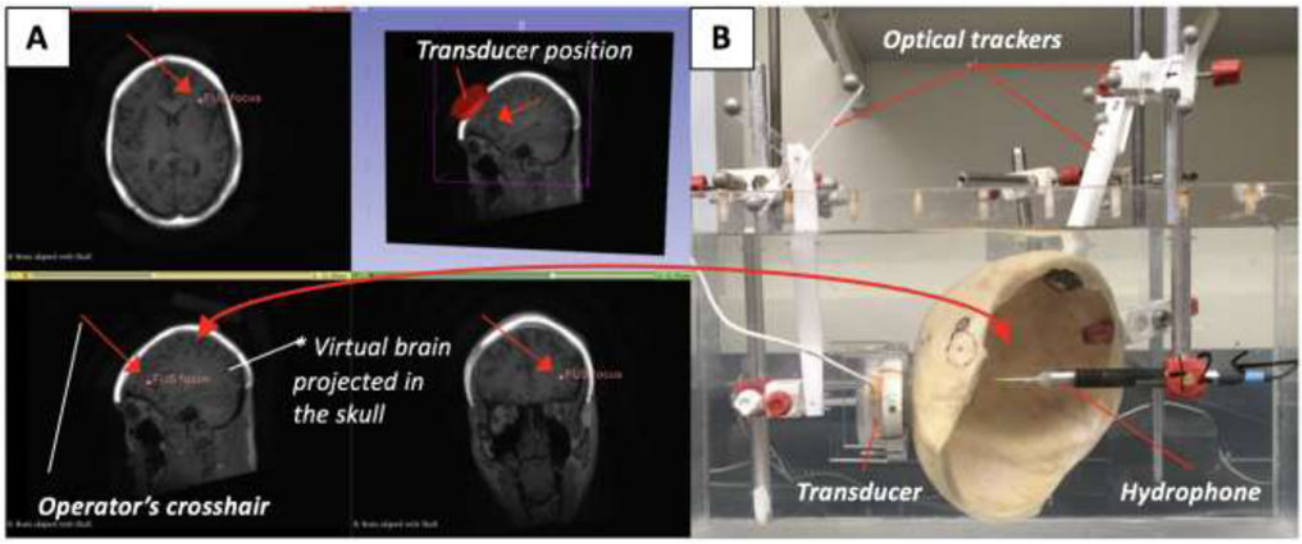

Fig. 1:

Experimental platform for the virtual brain projection method. **(A)** A brain MRI image volume is scaled to fit into a preserved human calvaria specimen's MRI image volume using 3D Slicer. **(B)** The transducer (3.25 cm focal length) and FUS focus are shown positioned to target the left DLPFC in the virtual domain. Real-time optical tracking of the transducer and hydrophone relative to the specimen in the physical domain during pressure field mapping. The red arrows in **(A)** point to the operator crosshair used to position the transducer onto the DLPFC.

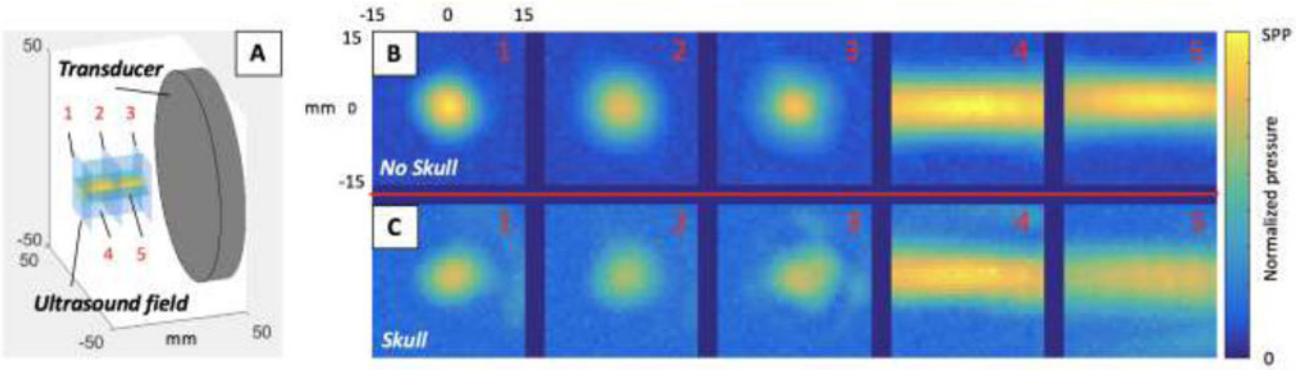

Fig. 2:

FUS pressure field mapping of the left DLPFC virtual target regions in the calvaria skull specimen using the 3.25 cm focal length transducer. **(A)** The orientation of the mapping planes relative to the transducer position. Pressure field maps in the axial (1, 2, 3) and longitudinal (4, 5) planes **(B)** with no skull in the beam path and (C) with the skull in the beam path when targeting the DLPFC of the virtual brain co-registered with the real skull.

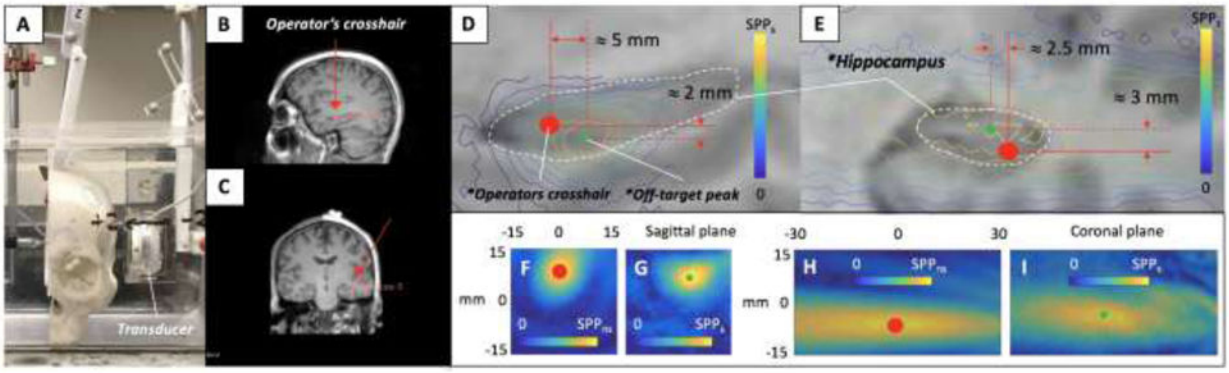

Fig. 3:

(A) The parasagittally sectioned skull specimen containing the left HPC virtual target using the 7.5 cm focal length transducer in the water tank. The operator's crosshairs are shown targeting the HPC in the **(B)** sagittal and **(C)** coronal MRI planes. **(D)** Contour map of the trans-skull FUS pressure field maps projected onto the virtual brain (sagittal plane of HPC enclosed with a white dotted line) for approximating the off-target peak as the operator used the crosshairs to target the HPC. **(E)** The same presentation as **(D)** but depicting the HPC in the coronal plane. FUS pressure field maps acquired **(F)** without and **(G)** with the skull in the sagittal plane and the equivalent acquisition in the coronal plane with **(H)** and **(I)**, respectfully.

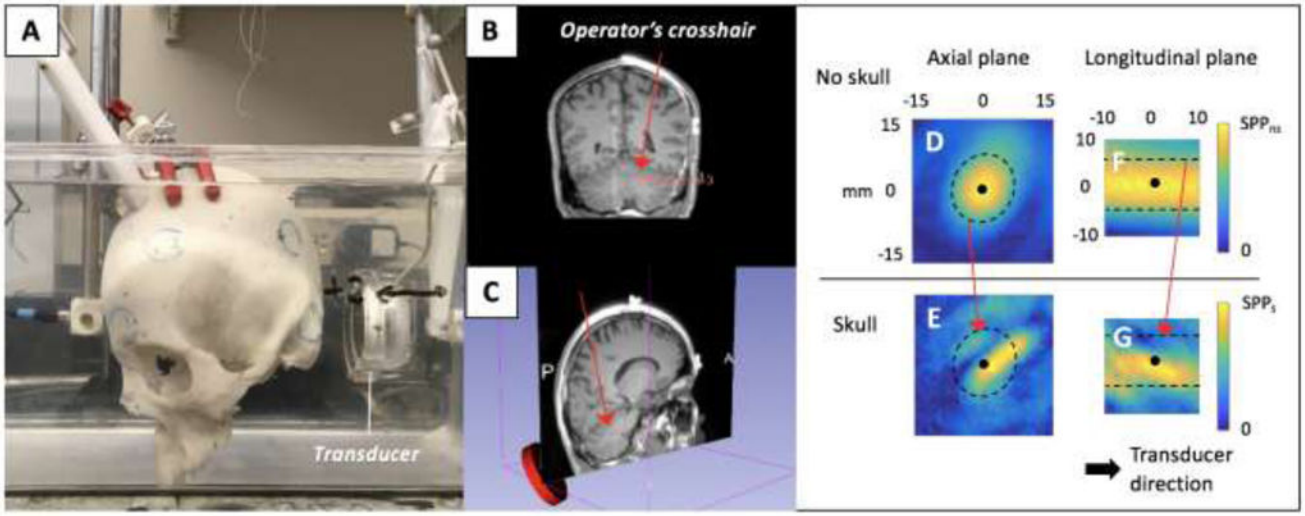

Fig. 4:

The parasagittally sectioned skull specimen containing the **(A)** CBM-VER virtual target with the 7.5 cm focal length transducer in the water tank and **(B)** operator positioning the crosshair on the CBM-VER virtual target. The FUS pressure field maps acquired in the FUS focal region, with and without skull. FUS pressure field maps acquired **(D)** without and **(E)** with the skull in the axial plane of the transducer and the equivalent acquisition in the longitudinal plane with **(F)** and **(G)**, respectfully. The black dot and black dotted line in **(D, E, F, & G)** represent the approximate spatial peak of the FUS pressure field (with no skull obstruction) and all pixels inside the boundary line contain values approximately half of the spatial peak value.